Mon. Not. R. astr. Soc. (1981) **194**, 967–986

The evolution of viscous discs – I. Mass transfer variations

G. T. Bath *Department of Astrophysics, South Parks Road, Oxford OX1 3RQ*
J. E. Pringle *Institute of Astronomy, Madingley Road, Cambridge CB3 0HA*

Received 1980 August 6; in original form 1980 June 4

Summary. A method for treating the time-dependent evolution of accretion discs in mass-transferring binaries is described. We apply the method to study the evolution into a steady disc following turn-on of mass transfer at a constant rate on to a white dwarf. The final steady-state is in agreement with analytic α-disc solutions. The effect of high mass-transfer-rate bursts by the companion star is studied, and compared with the eruptions of dwarf novae. We conclude that the overall outburst properties of dwarf novae are satisfactorily reproduced by bursting mass-transfer and that $\alpha \sim 1$ for this model.

1 Introduction

Accretion discs play a major role in many models of quasars and active galactic nuclei, and are a natural consequence of mass transfer in a number of interacting binary stars. In spite of their popularity, the physics of a major part of accretion-disc theory – the nature of the viscosity – remains unknown. An observational approach to the problem seems more likely to yield results than a purely theoretical one, and for this reason we have begun an investigation of models of time-dependent disc behaviour. The observations we have in mind for comparison with theoretical models are those of the cataclysmic variables. The reasons for studying the cataclysmic variables, and for considering in particular the outburst behaviour of the dwarf novae, are as follows:

(i) Accretion discs are actually observed in cataclysmic variables; in some of them the energy output at all wavelengths is dominated by the accretion process.

(ii) Much of the radiated energy from the disc (as opposed to the boundary layer) is emitted at observable wavelengths (> 1200 Å).

(iii) Time-dependent disc behaviour is determined by the magnitude of the viscosity. In contrast, in a steady disc the observable properties are fairly insensitive to the magnitude of the viscosity.

(iv) The outbursts of dwarf novae are generally considered to be powered by fluctuations in the accretion process.

(v) Modelling of discs in cataclysmic variables is simplified by being able to use the thin-disc approximation, since radiation pressure is unimportant.

Our approach is to construct models for the time-dependent behaviour of accretion discs relevant to the cataclysmic binaries, and to compare them with observational data. Since the viscosity is unknown, we parametrize our lack of knowledge by using the α-prescription proposed by Shakura & Sunyaev (1973). We aim to use comparison with observations to restrict possible values of α. At this stage a more sophisticated approach is not warranted by the data.

In Section 2 we describe the basis of the method used, and apply it in Section 3 to the evolution of a disc towards a steady state. The final steady state is compared to analytic results. In Section 4 we examine the effects on the structure of the disc of bursts of mass transfer from the companion star. In Section 5 we compare the resulting behaviour with dwarf nova eruptions. In Section 6 we experiment with changing the time structure of the mass-transfer bursts and with varying the parameters of the binary system.

2 The basic equations

Our treatment of the time-dependent behaviour of the disc is essentially the same as that employed in previous studies. It most closely parallels the approach of Lightman (1974a,b) in that we adopt the α-prescription for viscosity proposed by Shakura & Sunyaev (1973).

2.1 DERIVATION OF EQUATIONS FOR DISC EVOLUTION

We make the usual assumption that the thickness of the disc, $2H$, is everywhere small compared to its radius, R. This assumption is justified *a posteriori* from inspection of the models we produce. We neglect the effect of the secondary star on the motion of the disc around the primary, mass M_1, except insofar as we take account of the tidal effect of the secondary in limiting the size of the disc (see Section 2.2). This assumption holds to a good approximation (Papaloizou & Pringle 1977). These two assumptions imply that the azimuthal velocity, v_ϕ, in the disc is Keplerian, so that

$$v_\phi = R\Omega = (GM_1/R)^{1/2}. \tag{2.1}$$

The equation of hydrostatic equilibrium in the direction perpendicular to the disc (the z-direction) now gives $H/R \sim c_s/v_\phi$, where c_s is the sound speed on the $z = 0$ plane. We assume further that the radial flow velocity is very subsonic (see below for justification).

The equation for mass conservation is

$$\frac{\partial \Sigma}{\partial t} + \frac{1}{R}\frac{\partial}{\partial R}(R\Sigma v_R) = 0, \tag{2.2}$$

where Σ is the surface density of the disc. Similarly the equation for conservation of angular momentum is

$$\frac{\partial}{\partial t}(\Sigma R^2\Omega) + \frac{1}{R}\frac{\partial}{\partial R}(R\Sigma v_R R^2\Omega) = \frac{1}{R}\frac{\partial}{\partial R}(R^2 W), \tag{2.3}$$

where W is the z-integrated shear stress. If the kinematic viscosity is ν we may write

$$W = -\nu\Sigma R\frac{d\Omega}{dR} \tag{2.4}$$

and equations (2.2)–(2.4) can be combined to give

$$\frac{\partial \Sigma}{\partial t} = \frac{3}{R}\frac{\partial}{\partial R}\left[R^{1/2}\frac{\partial}{\partial R}(\nu \Sigma R^{1/2})\right]. \tag{2.5}$$

This is the basic equation which describes the evolution of the disc due to viscous processes.

2.2 DISC STRUCTURE IN THE z-DIRECTION

The α-prescription for the viscosity is simply the assumption that $\nu \lesssim c_s H$ (Shakura & Sunyaev 1973). Formally this may be written $W = 2H\alpha P$, where P is the pressure in the disc. Using this, together with the equation of state

$$P = \frac{\mathscr{R}\Sigma T}{\mu 2H} + \frac{1}{3}aT^4, \tag{2.6}$$

where T is the disc temperature (on the $z = 0$ plane), and the equation of hydrostatic equilibrium in the z-direction, which can be written

$$P = \frac{1}{2}\Sigma H\left(\frac{GM_1}{R^3}\right), \tag{2.7}$$

then equation (2.4) becomes

$$\nu = \frac{2}{3}\alpha H^2 \Omega. \tag{2.8}$$

The energy generated in the disc due to viscous dissipation is assumed to be radiated locally. For α-discs this is a good approximation since the inflow velocity is so small. Energy is deposited locally in the disc at a rate $2F$ where

$$F = \frac{1}{2}\nu\Sigma\left(R\frac{d\Omega}{dR}\right)^2 = \frac{9}{8}\nu\Sigma\frac{GM_1}{R^3} \tag{2.9}$$

in units of energy per unit area per unit time. This is assumed to be equal to the rate at which energy diffuses out of one side of the disc which is in local thermodynamic equilibrium, so that we may write

$$F = \frac{2acT^4}{3\Sigma\kappa} \tag{2.10}$$

where $\kappa(\rho, T)$ is the opacity. Similarly, the effective temperature at the surface of the disc is

$$T_e = \left(\frac{4F}{ac}\right)^{1/4}. \tag{2.11}$$

Using these equations, it is easy to verify that the relevant disc time-scales, which are (i) the dynamical time-scale $t_\phi = \Omega^{-1}$, (ii) the z-time-scale $t_z = H/c_s$, (iii) the thermal time-scale $t_{th} = \Sigma c_s^2/F$, and (iv) the viscous time-scale $t_\nu = R/v_R \sim R^2/\nu$, are ordered such that $t_\phi \simeq t_z \lesssim t_{th} \ll t_\nu$ (Pringle 1976). This justifies our procedure of treating the structure of the disc in the z-direction as in mechanical and thermal equilibrium at each stage of a slow viscous evolution in the radial direction.

To complete the set of equations, we assume that the opacity is given by Kramer's opacity law and take

$$\kappa = 0.4 + 3.2 \times 10^{22} \frac{\Sigma}{HT^{3.5}} \text{ cm}^2 \text{ g}^{-1}. \tag{2.12}$$

Below $T = 10^4$ K this formula is not valid since, for $T \lesssim 10^4$ K, hydrogen recombination leads to a rapid drop in opacity. For $T \lesssim 10^4$ K, we take $\kappa = 0.4 \text{ cm}^2 \text{ g}^{-1}$. We defer discussion of the implications of this until later.

2.3 BOUNDARY CONDITIONS AND SOURCE TERMS

The solution of equation (2.5) requires boundary conditions at the inner and outer radii of the disc. At the inner radius $R = R_1$, we allow any material there to be accreted on to the central star and set $\Sigma = 0$. This also ensures that the viscous torque acting on the disc due to the central star is zero (Pringle 1977). At the outer edge of the disc in a close binary system, tidal effects due to the secondary star remove angular momentum efficiently from the disc material and limit the disc radius to about 0.8–0.9 of the size of the primary's Roche lobe (Lin & Pringle 1976; Papaloizou & Pringle 1977). Thus an appropriate boundary condition is to fix the outer radius $R = R_N$ and to take $\partial \Sigma / \partial R = 0$ at that point. This ensures $v_R = 0$ at $R = R_N$, and removes angular momentum from matter at that radius at the required rate.

We wish to consider the effect on disc structure of mass transfer from the secondary. The matter transferred from the secondary is added to the disc at the outer radius, but has specific angular momentum around the primary of $h = (GM_1 R_K)^{1/2}$ where $R_1 < R_K < R_N$. Thus the additional material does not have enough angular momentum to orbit at the outer radius R_N. We assume that this material mixes and shares its angular momentum with the matter in the disc and that the mixing occurs on a dynamical time-scale. The exact description of the mixing process is given in Section 2.4.

2.4 NUMERICAL PROCEDURE

We change variables to $X = 2R^{1/2}$ and $S = X\Sigma$, and rewrite equation (2.5) in the form

$$\frac{\partial S}{\partial t} = \frac{12}{X^2} \frac{\partial^2}{\partial X^2} (S\nu). \tag{2.13}$$

We use a grid of N radius zones (usually $N = 20$) with equal spacing ΔX in the spatial variable X.

The numerical solution of disc evolution occurs in three stages for each time step, Δt. Given a disc structure at time t, we first add an appropriate amount of mass at the outer radius. Secondly we use equation (2.13) to calculate the new surface-density distribution at time $t + \Delta t$. Thirdly we recalculate the disc structure in the z-direction. We consider each stage in turn.

Stage I – Addition of mass at the outer radius

If the mass transfer rate is $\dot{M}(t)$, the total mass added in each time-step is $\Delta M = \dot{M} \Delta t$ with associated angular momentum $\propto 2\Delta M R_K^{1/2} = \Delta M X_K$. Suppose at the ith time-step a mass ΔM^i is added to the outermost zone X_N, in which the zone mass is $\Delta M_N^i = \pi S_N^i X_N^2 \Delta X / 4$.

The total mass $\Delta M^i + \Delta M_N^i$ has a combined angular momentum which puts it into a new orbit with a corresponding value of X given by

$$D_N = \frac{X_K \Delta M^i + X_N \Delta M_N^i}{\Delta M^i + \Delta M_N^i}. \tag{2.14}$$

If $D_N < X_{N-1}$, mixing with the $(N-1)$th zone occurs and the process is repeated, and subsequently for succeeding zones, until the Jth zone is reached for which

$$D_J = \frac{X_K \Delta M^i + \sum_J^N X_n \Delta M_n^i}{\Delta M^i + \sum_J^N \Delta M_n^i} > X_{J-1}.$$

In this way the stream continues to penetrate, with the addition of swept-up disc material, until the resulting orbital radius is greater than that of the next adjacent $(J-1)$th zone. The total mass is then shared between the $(J-1)$th and Jth zone such that angular momentum is conserved. This is satisfied by distributing the total mass as $\overline{\Delta M_{J-1}^i}$ and $\overline{\Delta M_J^i}$, where

$$\overline{\Delta M_J^i} = \frac{X_J - D_J}{X_J - X_{J-1}} \left(\Delta M^i + \sum_J^N \Delta M_n^i \right)$$

$$\overline{\Delta M_{J-1}^i} = \frac{D_J - X_{J-1}}{X_J - X_{J-1}} \left(\Delta M^i + \sum_J^N \Delta M_n^i \right) + \Delta M_{J-1}^i. \tag{2.15}$$

The new surface density and values of S_J^i and S_{J-1}^i in these zones are determined and advanced in time in the usual way.

In addition to feeding mass into the disc, the incoming stream dissipates potential energy. In dwarf nova systems, this energy is liberated in the bright-spot region. We include this contribution by adding a source term, Y, in the energy equation for the disc (equation 2.9) in the two disc zones at R_{J-1} and R_J. In these zones

$$Y_{J-1} = \frac{GM_1\dot{M}}{2\pi R_{J-1}^2 \Delta R_{J-1}} \frac{\overline{\Delta M_{J-1}^i}}{\overline{\Delta M_{J-1}^i} + \overline{\Delta M_J^i}} \tag{2.16}$$

and similarly for the Jth zone. Using this procedure the bright-spot energy is included, but is smeared around the disc rim. Thus the energetics of the stream–disc interaction are included consistently but not the angular dependence. Properties such as the effective temperature, pressure etc. at the rim are therefore averages resulting from spreading the bright-spot completely round the disc.

Stage II – Evolution of surface density

We integrate equation (2.13) using the standard first-order explicit integration method. For the nth zone the new value of S_n after i time-steps is

$$S_n^{i+1} = S_n^i + \frac{12\Delta t}{X_n^2 \Delta X^2} (S_{n-1}^i \nu_{n-1}^i + S_{n+1}^i \nu_{n+1}^i - 2S_n^i \nu_n^i), \tag{2.17}$$

where the time-step Δt is required for stability to satisfy

$$\Delta t < \frac{1}{2} \frac{X_n^2 \Delta X^2}{12\nu_n}. \tag{2.18}$$

Stage III – The z-structure

Once the surface density is determined, equations (2.6)–(2.11), together with additional energy input described by equation (2.16), provide a complete definition of the rest of the disc parameters. These equations are solved at each grid point using a Newton–Raphson iterative procedure.

3 The development of a steady disc

We now test the method outlined above by commencing from a state in which the disc contains zero mass (though, in practice, for numerical reasons the initial grid contains a small

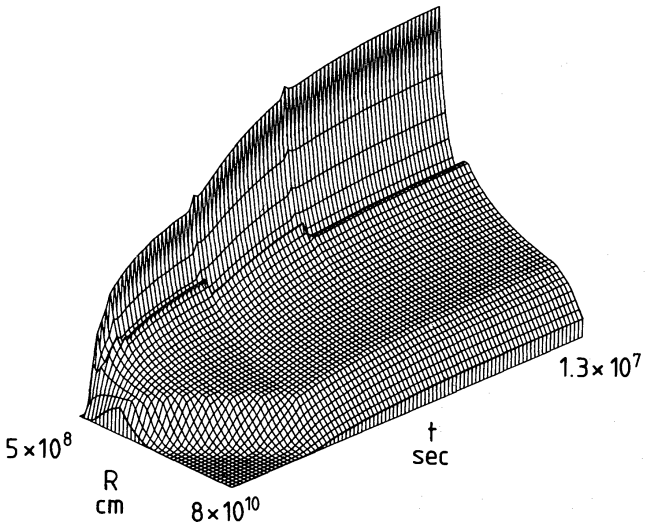

Figure 1. Surface-density evolution with constant mass-transfer. The radial surface-density distribution is plotted as a function of time. Mass transfer commences at $t = 0$ and continues at a constant rate of 5×10^{16} g s^{-1}. Matter initially orbits in a ring at 2×10^{10} cm and spreads out into a steady disc after $\sim 10^7$ s with a maximum value at the inner radius of $\Sigma = 40$ g cm^{-2}.

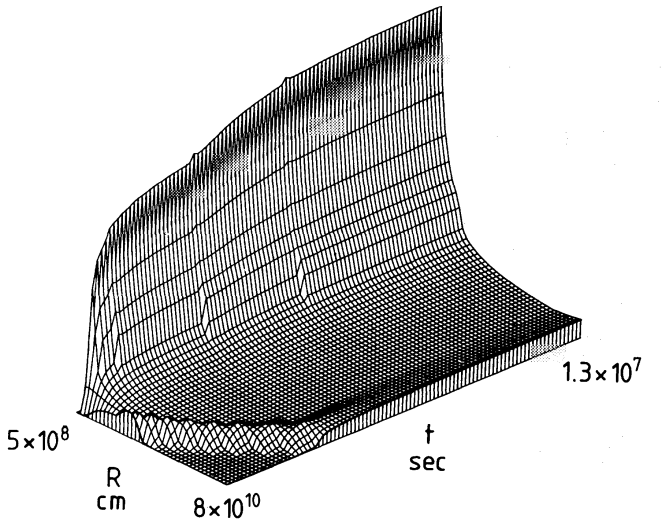

Figure 2. Temperature evolution. The central disc temperature (in the $z = 0$ plane) is plotted as a function of radius and time. The bright-spot forms a high temperature ridge on the outer edge of the disc, which expands out to the tidal radius after $\approx 3 \times 10^6$ s. This is followed by evolution to a steady state with a maximum temperature, $T = 5.0 \times 10^4$ K, in the innermost zone.

amount of low-density gas) and, in time, a constant stream of matter from the secondary builds up a steady accretion disc. Since we are interested in applying our results to accretion discs in cataclysmic variables, we take $M_1 = 1M_\odot$, $R_1 = 5 \times 10^8$ cm, R_N in the range $2–8 \times 10^{10}$ cm, and $\dot{M}$ in the range $10^{16} – 10^{17}$ g s^{-1}. We take $\alpha = 0.4$ and choose a value of R_K appropriate to a binary with mass ratio, $q = 1$ (Lubow & Shu 1975). The effects of changes in α and R_N are discussed at the end of this section and in Section 6.

The evolutionary behaviour of a typical model is shown in Figs 1–3, for which $R_N = 8 \times 10^{10}$ cm, $R_K = 2.1 \times 10^{10}$ cm, and $\dot{M} = 5 \times 10^{16}$ g s^{-1}. Evolution to the steady state occurs in $\approx 10^7$ s. The surface-density plot (Fig. 1) shows that a ring, formed initially at $R = R_K$,

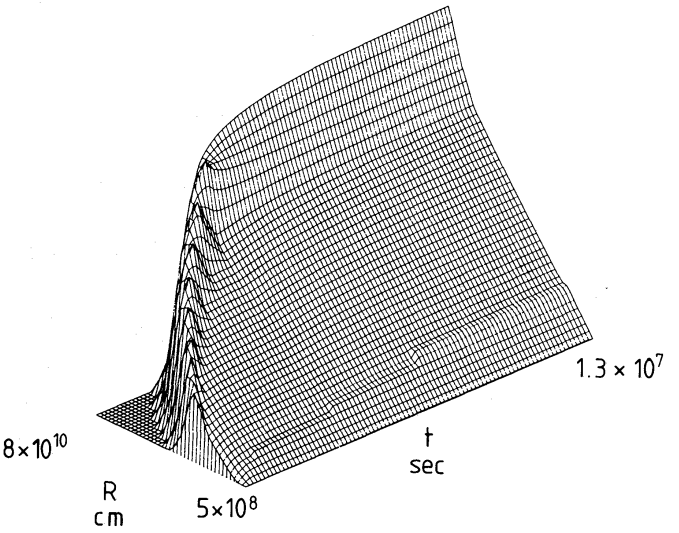

Figure 3. Disc semi-thickness as a function of time. The radius grid is reflected (relative to Figs 1 and 2) to place the stellar surface to the right and the tidal radius to the left in the R coordinate. Disc expansion leads to a steady-state structure. At the tidal radius the bright-spot produces thickening of the disc. The maximum value of $H = 2.1 \times 10^9$ cm and the disc remains thin throughout, with $H/R \approx 2.5 \times 10^{-2}$ at all radii.

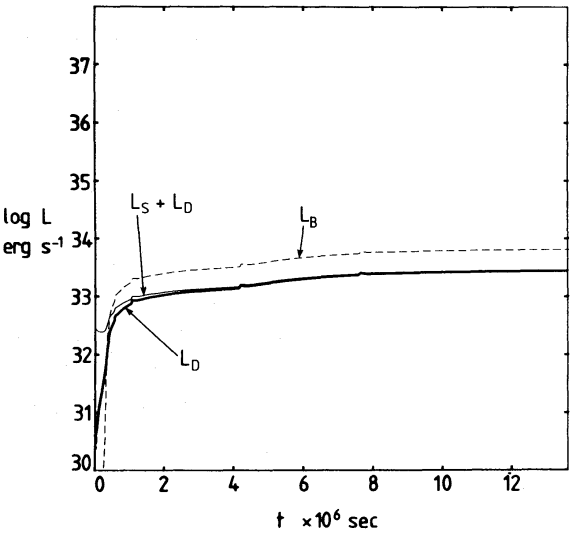

Figure 4. Variation of luminosity of one disc face, L_D, of spot (total) and disc luminosity, $L_S + L_D$, and total boundary-layer luminosity, L_B, with time. The spot luminosity dominates until viscous evolution spreads the initially formed ring out into a disc. Both L_D and L_B then rise asymptotically toward their steady-state values. Note that the slight glitches are due to the discontinuity in the assumed opacity law at $T = 10^4$ K and are unphysical.

rapidly spreads out (*cf.* Lynden-Bell & Pringle 1974; Lightman 1974b). After 2×10^5 s the ring reaches the inner boundary and accretion on to the white dwarf begins. After 3×10^6 s the ring spreads out to the outer tidal radius. From then on, the disc evolves towards a steady state with surface density increasing over the whole disc. The rate of inward mass-transport increases, until a final steady state is achieved when the mass flux on to the central star balances the mass-transfer rate of 5×10^{16} g s^{-1}.

Changes in central ($z = 0$) temperature are shown in Fig. 2. The initial ring-expansion is clearly delineated by the behaviour of the bright-spot, which is pushed out to the outermost grid point as disc structure develops. Once accretion on to the white dwarf has started, temperatures in the inner parts of the disc rise rapidly to a steady-state maximum of 5×10^4 K. The cool outer-disc region is at a temperature $< 10^4$ K and, as stated previously, the opacity in these regions is poorly treated. The bright-spot forms a prominent higher temperature ridge on the outer edge. Note that, since the stream/disc dissipation region has been spread round the entire rim of the disc, the temperature here does not reflect the true bright-spot value, but is an average over the spot and surrounding disc at that radius.

In the high-temperature region, $T > 10^4$ K, the optical depth through the disc, $\tau > 30$, and all the assumptions of the model are satisfied. In the cooler outer region, τ drops to values as low as 3 and details of the resulting structure are questionable (though note that τ increases for models with lower α discussed below).

The disc semi-thickness is shown in Fig. 3 (where the radius coordinate has been inverted to show the structure of the inner disc region). Development from a ring to a disc configuration is evident, with a final steady-state distribution which thickens almost linearly towards the outer edge (in agreement with α-disc models). A maximum disc-height of 2×10^9 cm occurs in the spot region on the outer edge.

As the mass flux through the disc builds up, so the integrated luminosity rises asymptotically towards the final steady-state value. The growth of disc luminosity, and of disc plus bright-spot, is shown in Fig. 4. We plot the integrated luminosity radiated through *one* side of the disc, L_D, and (half) disc plus total spot luminosity $L_S + L_D$. Initially the spot dominates as an energy source. As disc structure is established, and the mass flux through the central regions and on to the white dwarf grows, so the disc becomes the dominant energy source with a final ratio of luminosities, $L_S/L_D \sim 2R_N/R_1 \sim 300$.

Also shown is the *total* boundary layer luminosity, L_B (Pringle 1977). We plot the total boundary-layer luminosity rather than the visible luminosity, $L_B/2$, to obtain a clear separation between L_B and L_D in the diagram. Note how the mass flux on to the white dwarf grows once the ring spreads down to the stellar surface, to generate a final boundary luminosity, $L_B = 2L_D$ (the glitches in luminosity, and in other figures, are due to the assumed opacity behaviour at $T = 10^4$ K, and are unphysical).

We now compare the resulting disc with steady α-disc models. The final distribution of surface density, temperature and height is close to that of α-disc models. The differences are due to the assumed opacity dependence not being a single power-law.

The radiative flux distribution in a steady state is independent of both κ and ν, and is therefore a check on the final state of the time-dependent calculations. The inner boundary condition we have used corresponds to the case in which the accreting star exerts no torque on the disc. In this case the steady-state flux from one side of the disc is given by

$$F = \frac{3GM_1\dot{M}}{8\pi R^3}\left[1 - \left(\frac{R_1}{R}\right)^{1/2}\right]. \tag{3.1}$$

This is compared with a typical time-dependent model in steady conditions in Fig. 5. Points are the computed flux value at each grid point and the continuous curve equation

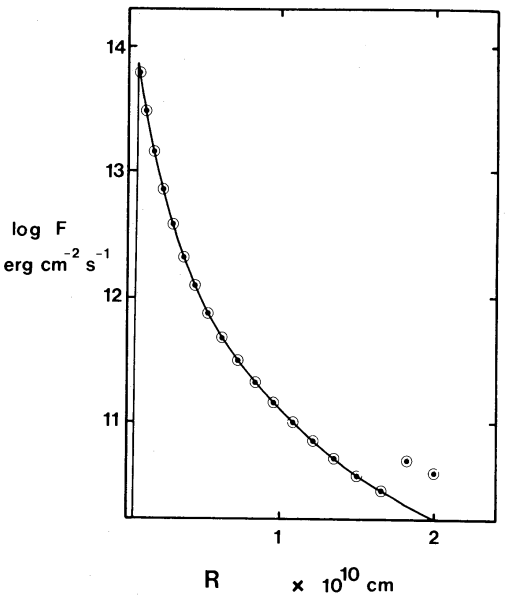

Figure 5. Energy emitted per unit surface area per second from the disc surface as a function of radius for steady conditions. We compare the analytic solutions (continuous curve) with values in each zone of a numerical model evolved to a steady state (circled dots). The model shows close agreement except in the two outer zones (in this model at 2×10^{10} cm) where the bright-spot energy enhances the flux above the standard analytic solution.

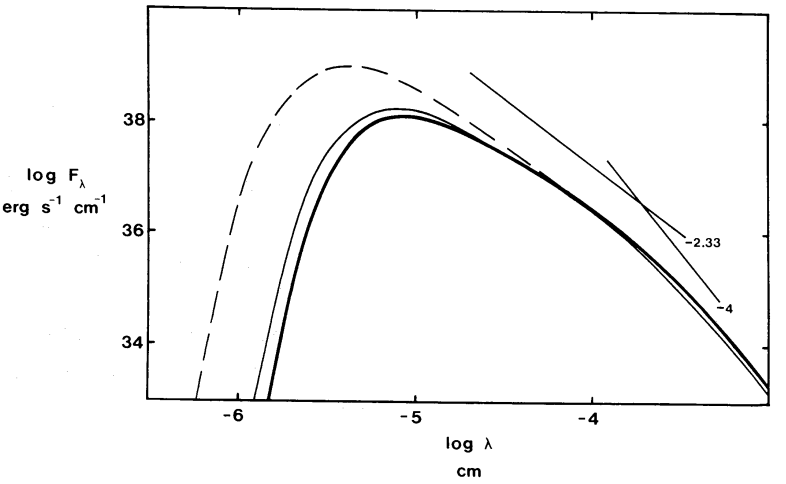

Figure 6. Spectral distribution of a steady disc for the following conditions: (1) continuous thick line – numerical model evolved to a steady state; (2) continuous thin line – analytic solution for a steady disc with the same inner boundary condition as (1); (3) broken line – steady disc with $F = 3GM\dot{M}/8\pi R^3$.

The integrated disc spectrum has a slope -2.33 in case (3), and tends to this slope at optical wavelengths in case (1) and (2). In these cases, Keplerian motion at all disc radii leads to flattening of the spectrum to ≈ -2.0 as the Wien turnover is approached. The numerical model (case 1) is reduced below the analytic model (case 2) at short wavelengths, due to the finite size of the grid and consequent loss of resolution of temperature structure near the temperature maximum (see Fig. 5). The numerical model (case 1) is enhanced above the analytic model (case 2) at long wavelengths due to inclusion of the bright-spot energy.

(3.1). The bright-spot leads to higher fluxes in the two outer zones, but elsewhere the model closely follows the predicted distribution.

From the flux and effective temperature distribution we calculate the emergent spectrum, ignoring limb darkening, and assuming that the local continuum is Planckian. This is shown

in Fig. 6. Once again the numerical models are satisfactory. The spectrum is $F_\lambda \propto \lambda^{-\beta}$ with β approaching -2.33 at longer wavelengths. $\beta = 2.33$ is the predicted spectral index (Lynden-Bell 1969) for steady, blackbody discs which are large enough for boundary effects to be unimportant. This is shown in Fig. 6 by the dashed curve, which is the spectrum due to a flux distribution $F = 3GM_1\dot{M}/8\pi R^3$ and identical accretion rate and boundary radii.

Since the innermost grid point does not coincide with the temperature maximum in the disc at $R = 1.4R_1$, the model spectrum in the ultraviolet turns over to a Wien distribution at a somewhat longer wavelength than that based on equation (3.1). In the red region the spectrum is Rayleigh–Jeans ($F_\lambda \propto \lambda^{-4}$) and the spot luminosity enhances the flux of numerical models above that derived from equation (3.1).

We now compare models with different values of α, and examine the dependence of evolution time-scale and disc mass on the viscosity scaling-parameter. We define the time to achieve a steady state, t_{ss}, as the time to reach a surface accretion rate at R_1 within 0.1 per cent of the transfer rate. When we examine the effects of bursting mass-transfer, t_{ss} defined in this way is a measure of the characteristic decline time-scale of the disc outburst. The values of t_{ss} and the final disc mass, M_D, are given in Table 1, and t_{ss} is plotted against α in Fig. 7, for two values of R_N (2×10^{10} cm and 8×10^{10} cm), $R_K = 0.575R_N$, and $\dot{M} = 10^{16}$ g s^{-1}. Note the linear dependence of $\log t_{ss}$ on $\log \alpha$, with slope $-4/5$. This dependence agrees with that anticipated from steady-state models. The drift time-scale through a steady disc, $t_\nu \sim R/V_R \sim \alpha^{-1}(R/H)^2(R^3/GM)^{1/2}$. For these discs, steady-state models predict $H \propto \alpha^{-1/10}$ (Shakura & Sunyaev 1973), and $t_\nu \propto \alpha^{-4/5}$. The time to achieve a steady state in time-dependent models has the same dependence on α as the radial drift time-scale of the final steady disc.

Though we have defined t_{ss} as the time when $\dot{M}_1 = 0.999\dot{M}$, the same result is obtained for smaller values of $\dot{M}_1/\dot{M}$. So long as $\dot{M}_1 \sim \dot{M}$, the value of t_{ss} is not strongly sensitive to the way in which it is defined. Thus in these models $t_{ss}(\dot{M}_1 = 0.9\dot{M}) = 0.4t_{ss}(\dot{M}_1 = 0.999\dot{M})$. In contrast, if we define a response time, t_R, as the time for the disc luminosity to reach half the steady-state value, we find $t_R(\dot{M}_1 = 0.5\dot{M}) \approx 0.1\, t_{ss}(\dot{M}_1 = 0.999\dot{M})$. When we examine the effects of bursting mass-transfer, t_R defined in this way is a measure of the timescale associated with the rise in the light curve (so long as the mass-transfer rate in the burst increases on a shorter time-scale than t_R (see Section 6)).

From these results we find that, in order for the reaction time of the disc to be $10^5 - 10^6$ s, large viscosities are required with $1.0 > \alpha > 0.1$. The diffusion equation controlling mass transport in the disc leads to a rapid disc-response initially, followed by an asymptotic approach to a steady state on a longer time-scale.

Table 1.

	$R_N = 2\times10^{10}$ cm		$R_N = 8\times10^{10}$ cm	
α	t_{ss} (s)	M_D (g)	t_{ss} (s)	R_D (g)
3.16×10^{-1}	5.0×10^{6}	1.2×10^{22}	4.0×10^{7}	1.0×10^{23}
1.00×10^{-1}	1.2×10^{7}	2.9×10^{22}	1.1×10^{8}	2.5×10^{23}
3.16×10^{-2}	2.8×10^{7}	6.7×10^{22}	2.7×10^{8}	6.2×10^{23}
1.00×10^{-2}	6.0×10^{7}	1.4×10^{23}	7.0×10^{8}	1.5×10^{24}
3.16×10^{-3}	1.6×10^{8}	3.4×10^{23}	1.6×10^{9}	3.8×10^{24}
1.00×10^{-3}	3.9×10^{8}	8.5×10^{23}	4.0×10^{9}	9.2×10^{24}
3.16×10^{-4}	9.9×10^{8}	2.1×10^{24}	9.4×10^{9}	2.2×10^{25}
1.00×10^{-4}	2.5×10^{9}	5.4×10^{24}	1.9×10^{10}	4.8×10^{25}
3.16×10^{-5}	6.3×10^{9}	1.3×10^{25}		
1.00×10^{-5}	1.6×10^{10}	3.4×10^{25}		

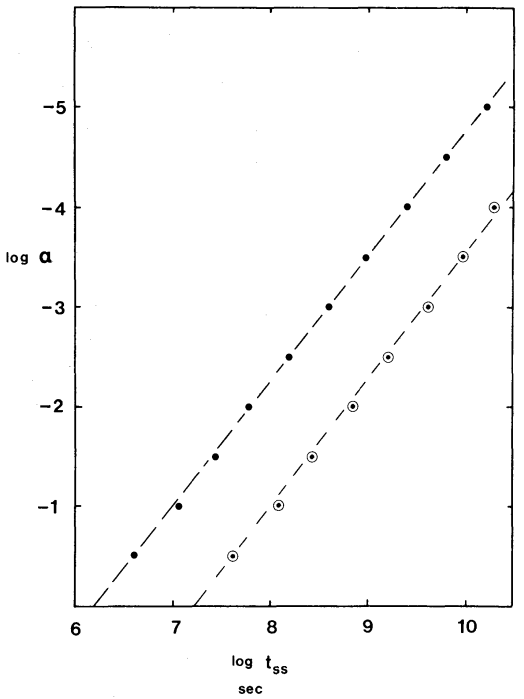

Figure 7. Dependence of disc evolution time for a fully formed disc on the viscosity parameter α. t_{ss} is defined as the time taken to achieve a stellar surface-accretion rate within 0.1 per cent of the mass-transfer rate and is a measure of the relaxation time, for example following an outburst. Dots are for outer disc radius $R_N = 2 \times 10^{10}$ cm and circled dots for $R_N = 8 \times 10^{10}$ cm. Mass transfer is at a rate $\dot{M} = 10^{16}$ g s^{-1}. Note that outburst decline times $\sim 10^6$ s require $10^{-1} < \alpha < 1$, and that t_{ss} is sensitive to the value of R_N.

4 Disc evolution with mass-transfer bursts: the basic model

As we stated in the introduction, dwarf novae provide an ideal test-bed for the application of time-dependent disc calculations for two reasons. First, their repetitive eruptions are caused by some quasi-periodic behaviour in the disc, almost certainly powered by accretion. Secondly, since the accretion energy is radiated primarily at ultraviolet and optical wave-

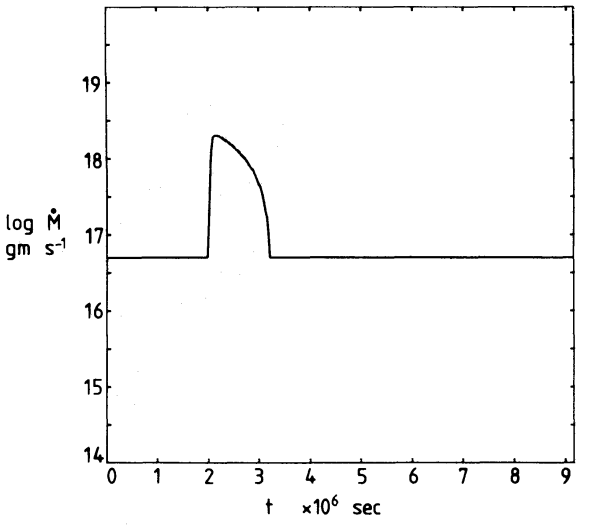

Figure 8. Mass-transfer rate changes in model 1. The background quiescent value is 5×10^{16} g s^{-1}. The rise and fall are linear in time and take 10^5 s and 10^6 s respectively.

lengths (with comparable emission at X-ray wavelengths, probably from the boundary layer), a large body of observational data exists to be fitted by any model. In this section we assume that α can be regarded as constant in both space and time, and examine some of the effects of variable mass-transfer caused, for example, by dynamical instabilities in the companion star (Bath 1975; Papaloizou & Bath 1975; Wood 1977). We defer discussion of variable viscosity and its possible role in dwarf nova eruptions to a subsequent paper.

In dwarf nova discs, the viscous time-scale at outburst is so fast that material diffuses down to the white dwarf surface in a time which is less than (or of the same order as) the rise-time of the outburst light-curve. The rise-time to maximum light is ~ 1 day in a normal outburst. The discussion concluding the previous section confirmed that α must be ~ 1 during the rise to achieve such short reaction times. Furthermore, only when $1.0 > \alpha > 0.1$ can a substantial mass of gas – sufficient to power dwarf nova eruptions – be transported from the

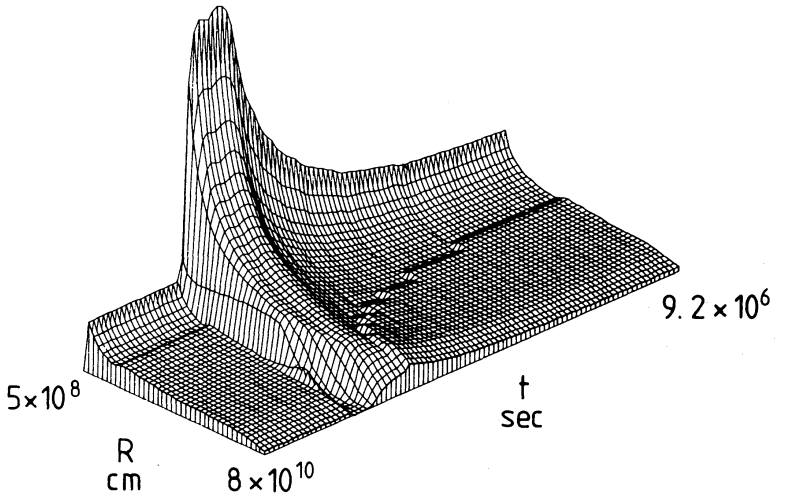

Figure 9. Surface density evolution of model 1. The increase in the mass-transfer rate at the start of the burst causes the initial steady disc to shrink as a result of the increased flux of low angular momentum material impacting on the outer rim. The surface density evolves toward a 'quasi-steady' distribution at a higher accretion rate and then relaxes back on a time-scale t_{ss} to the quiescent distribution. The maximum value of Σ at outburst is 240 g cm^{-2}.

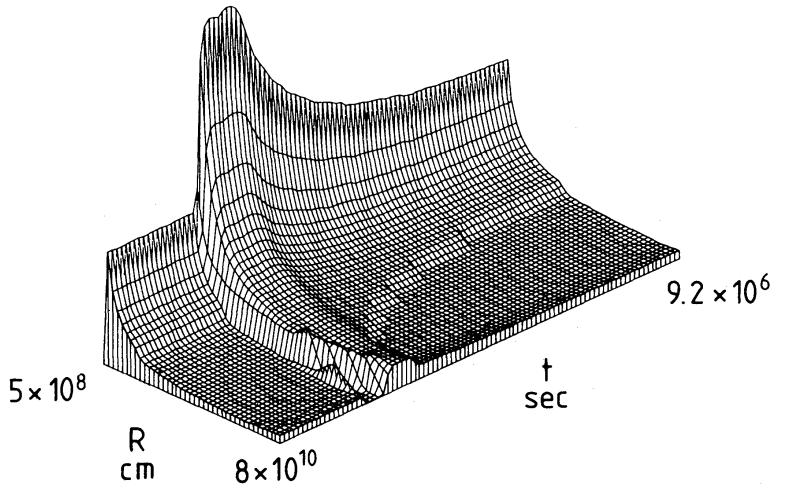

Figure 10. Evolution of central ($z = 0$) disc temperature during a mass-transfer burst (model 1). Initially the outer parts of the disc heat up, followed by relaxation towards a steady state, and cooling back to the quiescent distribution. The maximum value of the temperature at outburst is $T = 1.3 \times 10^5$ K.

outer regions of the disc to the white dwarf surface within the overall outburst time of $\lesssim$ weeks. In the following we take $\alpha = 0.4$.

We first describe the evolution of a basic model, whose overall characteristics are typical of dwarf nova eruptions, and in a later section consider results obtained with changes to this basic model. The basic model (model 1) is an attempt to fit a range of observed properties of outbursts of dwarf novae including the outburst luminosity range, colour changes through eruption cycle, optical and UV spectral behaviour, and X-ray properties. We stress, however, that the general features are insensitive to the detailed functional form of the transfer-rate variations. So long as the time-scale for changes is shorter than the viscous diffusion time-scale, the properties are roughly similar.

The transfer changes are given in Fig. 8. We take a rise and fall in $\dot{M}$ which is linear in time, with a rise-time 1×10^5 s, fall-time 1×10^6 s and a maximum value of $\dot{M}_{\rm max} = 2\times10^{18}\,{\rm g\,s^{-1}}$.

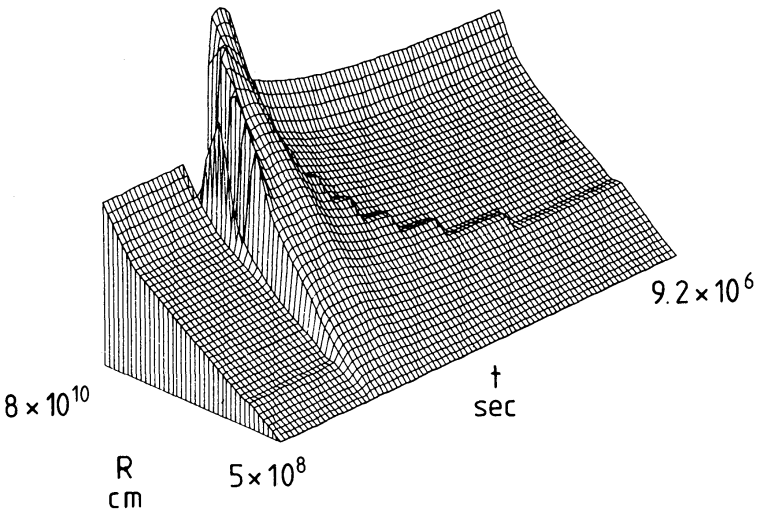

Figure 11. Evolution of disc semi-thickness during a mass-transfer burst (model 1) (R coordinate reversed). The disc contracts following the sudden influx of low angular momentum material and then expands more slowly out to the tidal radius. The maximum value of $H = 3.9\times10^9$ cm. Note that H changes by a factor $\lesssim 2$ with $\dot{M}$ changes of ≈ 40.

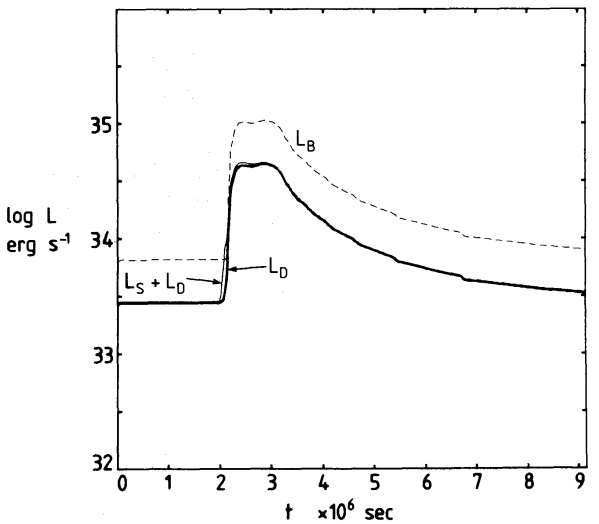

Figure 12. Variation of spot, disc and boundary layer luminosity during the mass-transfer burst (model 1). Both the rise and decay time-scales are determined by α, rather than the rate of change of $\dot{M}$.

The total burst mass is 1.17×10^{24} g. This compares with a quiescent disc mass of $M_D = 2.10 \times 10^{23}$ g.

The surface density evolution (Fig. 9) exhibits the following features, most of which are a consequence of the fact that a value of $\alpha = 0.4$ allows the disc eventually to adjust to a 'quasi-steady' structure at outburst. The initial rapid rise in the transfer rate causes the disc to contract, since the sudden large flux of low angular momentum material impacting on, and mixing with, lower density gas extending out to the tidal radius, reduces the orbital radius of the outer disc region. The surface density builds up to a ring-like structure, subsequently spreading out to the inner and outer boundary radii – evolving toward a higher density steady state. Following the fall-off to the quiescent $\dot{M}$ value, the disc relaxes to the original surface-density distribution, and recovers the initial quiescent structure.

The same general features are shown by the temperature changes (Fig. 10) – initial disc

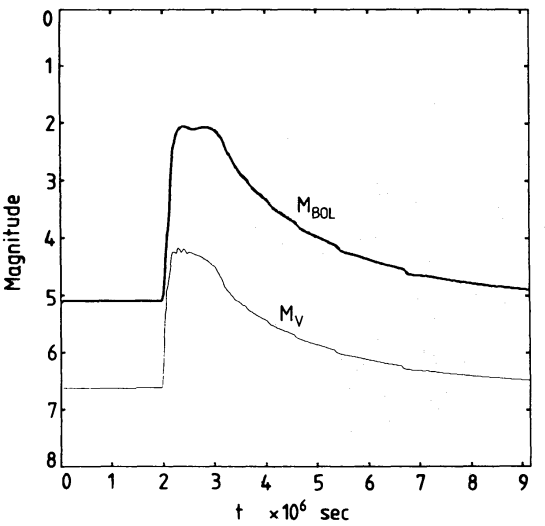

Figure 13. Outburst light curves of model 1, showing the characteristic rapid rise, flattened top, and slow decline of large-amplitude dwarf nova eruptions.

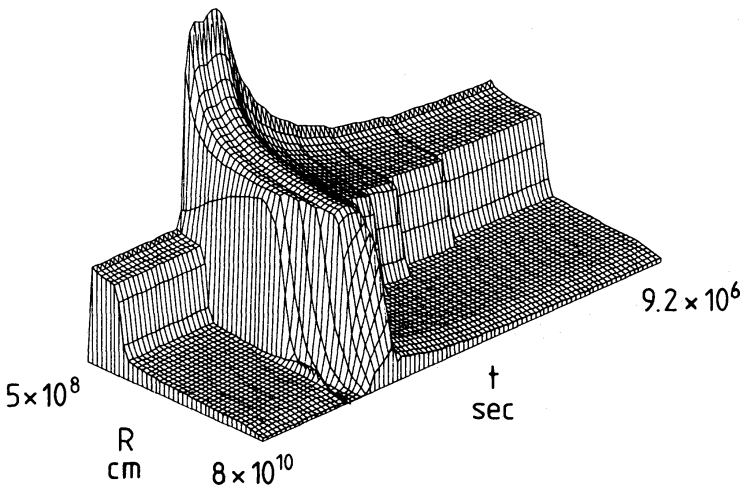

Figure 14. Variation of integrated optical depth, τ, through the disc as a function of time. In the quiescent state ($\dot{M} = 5 \times 10^{16}$ g s^{-1}), only the central regions of the disc are optically thick, and extended out to 2×10^{10} cm. In outburst, the optical thickness rises to values > 40 out to 7×10^{10} cm. The optically thick region then slowly contracts. The low values of τ might indicate that the outer parts are emission-line regions at quiescence.

contraction, rise to higher 'quasi-steady' temperatures, and a final slow decline. The semi-thickness evolution (Fig. 11) illustrates the initial contraction of the outer edge, followed by expansion and thickening.

The eruption light curve is shown in Fig. 12. For the assumed value of α and time-scale of the burst mass-transfer, the viscous time-scale (i.e. α) determines both the rise and decay time of the light curve. The disc and boundary layer luminosities are almost identical (we plot L_D through one disc face and the total boundary luminosity, L_B). The result that $L_B \sim 2L_D$ at all times reflects the fact that L_D is predominantly determined by the mass flux at R_1.

The bright-spot is strongly variable relative to the disc, and, unlike L_B, does not change in phase with L_D. It reflects the transfer rate at R_N rather than the accretion rate at R_1. We stress that the so-called bright-spot luminosity derived from the binary light-curve shoulder

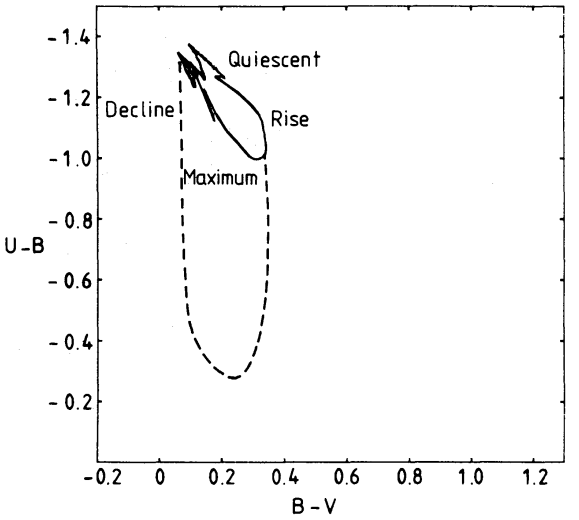

Figure 15. Behaviour in the two-colour diagram. The solid line is the loop obtained with integrated black-body emission, and the dotted line indicates the approximate extent of the loop if rough allowance for the Balmer jump is included.

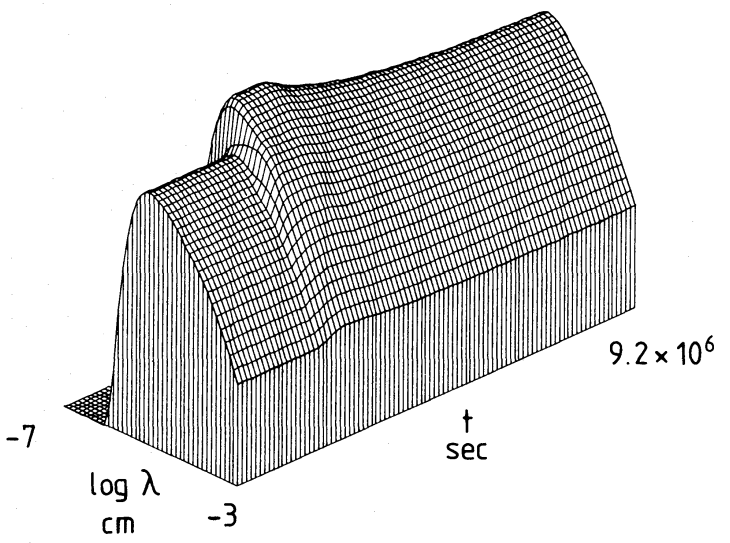

Figure 16. Variation of log F_λ during outburst, showing the initial reddening, followed by relaxation to the disc spectrum of Fig. 6.

(or bright-spot eclipse depth) in observed systems is not a measure of L_S but only a lower limit. It should not be compared with these theoretical curves without correction for the degree of anisotropy of the bright-spot radiation pattern.

5 Comparison with observations

Using simplifying approximations to the atmospheric structure of the disc, the model we have generated may be used as a diagnostic tool to interpret the observed eruption properties of dwarf novae. The primary data to be fitted are the visual light curve (Fig. 13), the integrated optical depth through the disc (Fig. 14), the evolution of the outburst in the two-colour diagram (Fig. 15), and the continuum spectral distribution (Fig. 16).

Before discussing these figures a number of qualifications are in order. The method is valid in those conditions for which our introductory assumptions of optical thickness, disc thinness, and thermal and dynamical time-scales are valid. In principle, given accurate opacities and a theory of viscosity, these assumptions can be rigorously checked and observed systems modelled. Our aim at this stage is less ambitious. To obtain results with reasonable computer run-times we have assumed a simple opacity law, and adopted a simple, widely used viscosity law. A number of the points made below are strongly influenced by these laws, and are therefore not to be regarded as established results, but rather as preliminary indications of how the observed data may be interpreted. With respect to the opacity, we have confirmed that the same qualitative features are produced with Cox–Stewart opacities. The main difficulty is calculating the opacity in the outer, cool ($T < 5000$ K) regions of the disc.

One of the major failings of the present model is its inability to treat optically thin conditions, since assumptions of local thermodynamic equilibrium, and radiative diffusion, then break down. As we show below, we anticipate that at low mass-transfer rates in the quiescent state, a large fraction of the outer part of the disc may be optically thin in the continuum. This is particularly the case in longer period systems, with large discs. We anticipate that this disc region will be an emission-line source (*cf.* Bath *et al.* 1974; Williams 1980; Mayo, Wickramasinghe & Whelan 1980), and a consistent treatment requires detailed balance calculations including time-dependent dissipative heating.

Here we calculate the disc spectrum by assuming that the disc is optically thick and blackbody everywhere, as described in Section 3. That is, we make no attempt to allow for the effects discussed above, and no attempt to calculate the atmospheric structure in the manner described by Mayo *et al.* (1980). Our results should accordingly be interpreted with caution. From the disc spectrum we calculate the flux in the *UBV* bands using the *UBV* response curves, and convert the flux to *UBV* magnitudes (Allen 1973).

We first compare the visual and bolometric light curves (Fig. 13) of the disc. We see that the initial rapid rise in the *V* band slows down as maximum light is approached, whilst the bolometric luminosity continues to rise rapidly. This is a consequence of the increasing fraction of radiation being emitted in the ultraviolet as the inner parts of the disc heat up (see Figs 10 and 16).

The associated optical thickness changes (Fig. 14) are large, and suggest important points to be borne in mind when interpreting eclipse observations of dwarf novae during outburst. The quiescent distribution has a discontinuous jump in τ – inner regions of the disc at $T > 10^4$ K are optically thick ($\tau \sim 40$) whilst outer regions have $10 > \tau > 1$ (though note that κ is arbitrarily defined in this outer region). During outburst the optically thick region expands to fill the whole grid, with $100 > \tau > 50$ through the bulk of the disc. The cause of this sudden increase in τ is two-fold. First, when the temperature rises above 10^4 K in any zone, a sudden increase in κ takes place, and second, as $\dot{M}$ increases, Σ increases. The primary mechanism is the first, i.e. the opacity change due to hydrogen ionization. The

τ-plot emphasizes an important aspect of dwarf nova disc-structure: the size of the disc which is optically thick does not reflect the density distribution directly (compare Figs 14 and 9).

When the burst is injected in the mass-transfer stream, the spectrum (Fig. 16) changes from a steady-state distribution. There is an initial reddening as the outer regions heat up, followed by a rise in the ultraviolet as the inner regions subsequently respond. At maximum light the continuum distribution is roughly that of a steady disc with a λ^{-2} spectrum extending into the far ultraviolet. During the decline the ultraviolet turnover shifts back to longer wavelengths. All these features are reflected inthe loop in the two-colour diagram (Fig. 15) – reddening on the rise, followed by migration up the blackbody line once the U spectral region is on the Rayleigh–Jeans part of the continuum, finally closing the loop as the λ^{-2} region migrates to longer wavelengths.

Interpretation of the two-colour diagram, and comparison of our models with the trajectory of observed dwarf novae, is not straightforward (*cf.* Mayo *et al.* 1980, for a discussion of the importance of atmospheric modelling in relation to the two-colour diagram). Probably the main error in our UBV values is due to ignoring the effects of the Balmer jump in both absorption and emission (Kiplinger 1980; Mayo *et al.* 1980). The contribution of the Balmer jump can be estimated by assuming that the Balmer jump is present in absorption when the bulk of the disc is optically thick and has the same effect on $U–B$ as it does in stars. Thus, we assume that the Balmer jump produces the same deficit in $U–B$ below a blackbody value as that in stars with the same $B–V$, but only when the disc is optically thick. The result is shown in Fig. 15.

The observed loop (*cf.* Bailey 1980; Mayo *et al.* 1980; Zuckermann 1962) shows the same general properties – reddening on the rise, followed by a blueward shift through B and U. At this stage we conclude that the two-colour trajectory is due both to initial enhanced dissipation in the outer disc regions, and to changes in the size of the Balmer jump (which is well-known to change from emission to absorption at outburst in some systems).

The X-ray observations (both hard and soft) of dwarf novae show considerable variations between systems (Córdova *et al.* 1980a; Córdova, Mason & Nelson, 1980b). Some are undetectable, others have comparable X-ray to optical/UV luminosity. We would anticipate the X-ray flux from the boundary layer to be anything up to a luminosity equal to the disc luminosity. The actual behaviour observed in any wavelength region depends rather critically, however, on changes in boundary layer conditions, which are uncertain (Pringle & Savonije 1979). The results of Córdova *et al.* (1980b) are in general agreement with the expectations of the model described.

6 Varying burst forms

The class of model we have treated, namely a bursting mass-transfer model, accounts for the differences in the light curve from outburst to outburst by variations in the burst amplitude and time-scale. Figs 17 and 18 show light curves of models with a variety of functional forms for the mass-transfer burst. Disc parameters are the same as the basic model (model 1). Model 2 (Fig. 17) has the same rise and decay time as the basic model, but a value $\dot{M}_{\max} = 5 \times 10^{17}\,\mathrm{g\,s^{-1}}$, a factor 4 times less than model 1. The reduced charge in the burst produces a lower amplitude outburst with no flat-top, and decay immediately following maximum light. The association of lower amplitude outbursts with an early decline from maximum, and of large outbursts with extended, flat-topped maxima, is a common characteristic of dwarf nova eruptions. This is particularly evident in those systems which show 'supermaxima'. Mayo *et al.* (1980) conclude that the mass flux is a factor 4 times

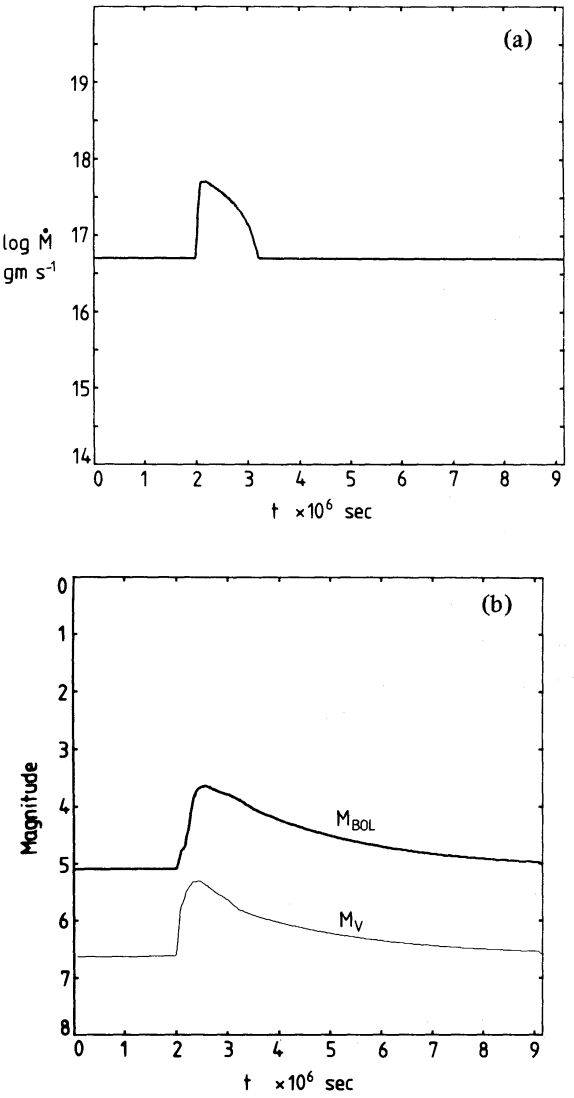

Figure 17. (a) Mass-transfer variation of model 2. The same time-dependence as model 1 is assumed, but $\dot{M}_{\max}$ is a factor 4 smaller, $5 \times 10^{17}\,\mathrm{g\,s^{-1}}$. (b) Outburst light curves of model 2. The lower burst-mass leads to a lower amplitude outburst, and a more rounded, shorter maximum.

larger in supermaxima outbursts. Models 1 and 2 are rough approximations with a time-dependent code to 'superoutbursts' and normal outbursts.

The increase in density and temperature in model 2 is less than model 1, and, as a consequence, model 2 experiences only a modest expansion of the optically thick inner region.

Model 3 (Fig. 18) is an example in which the rise time of the mass-transfer burst is longer than the diffusion time through the disc. As a consequence the rise is slow. Extended mass-transfer at a value $\dot{M}_{\max} = 5 \times 10^{17}\,\mathrm{g\,s^{-1}}$ leads to an extended, rounded maxima, of larger amplitude than model 2. The slower increase in the mass-transfer rate allows the disc to relax to a quasi-steady state even during the rise to maximum light. As a result the spectrum remains close to a steady distribution, and the loop in the two-colour diagram is considerably reduced. This agrees with the slow rise-time, 'anomalous', outbursts which Bailey (1980) notes do not have large $U-B$ changes at outburst. The suggestion that this is due to the mass-transfer rate increasing on a longer time-scale than the disc diffusion time-scale is supported by these calculations.

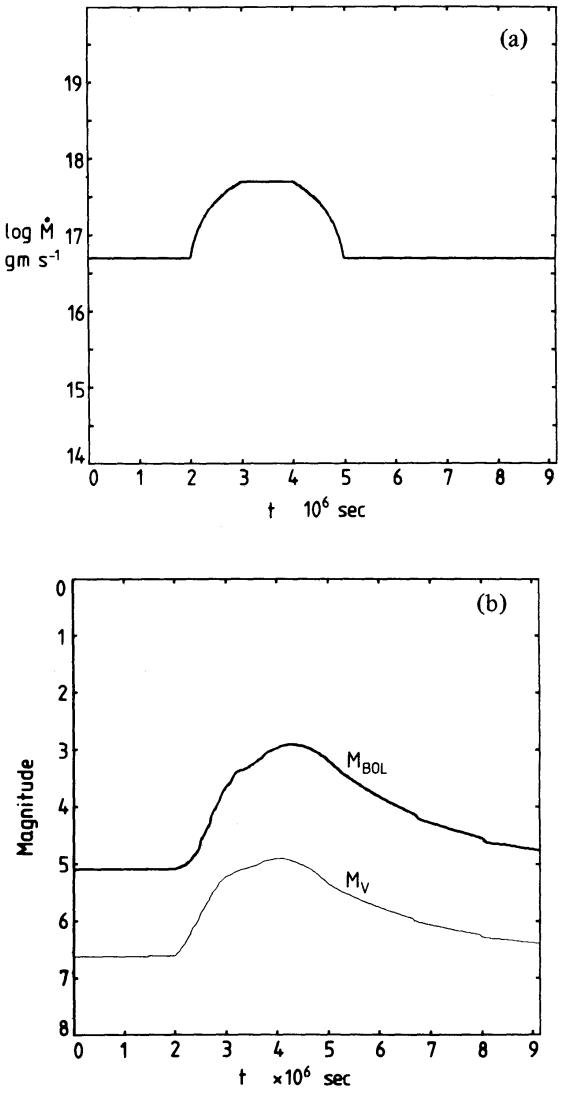

Figure 18. (a) Mass-transfer variation of model 3. $\dot{M}_{max} = 5 \times 10^{17}\,g\,s^{-1}$, but the rise time is 10 times longer than model 2, and is followed by an extended phase at maximum mass-transfer. (b) Outburst light curve of model 3. Variations in $\dot{M}$ now occur more slowly than the disc response-time, and the rise time is determined by the rate of increase of $\dot{M}$. The disc approximates a steady-state structure throughout the evolution and there is little reddening on the rise.

There are two factors, in addition to the form of the mass-transfer burst, which affect the outburst light-curve. These are the value of α. and the size of the disc. As discussed in Section 3, the diffusion time-scale varies as $\alpha^{-4/5}$. For $\alpha \leqslant 1$ the outburst time-scales cannot be reduced by a factor < 0.5 below those in the model presented here. In order to model outbursts with the shortest observed time-scales, ~ few days, small discs must be invoked. The diffusion time in a steady disc varies as $R^{3/2}$, and this is roughly the way in which the steady-state evolution time varies with R_N (see Table 1). Outburst times as short as a few days are obtained with tidal disc radii $\approx 10^{10}$ cm.

Bailey (1975) (see also Bath 1976) has pointed out that there is a rough correlation between the outburst decay time and the binary period. Systems with longer periods have long decay times after maximum. Since long-period systems transfer mass with higher specific angular momentum, and have larger tidal radii, this relationship suggests that the primary factor generating different outburst time-scales in different systems is the disc size

and not variations in the magnitude of viscosity. Our results confirm this and indicate that the viscosity is high, $\alpha \sim 1$.

References

Allen, C. W., 1973. *Astrophysical Quantities,* 3rd edn, Athlone Press, London.
Bailey, J., 1975. *J. Br. astr. Ass.*, **86**, 30.
Bailey, J., 1980. *Mon. Not. R. astr. Soc.*, **190**, 119.
Bath, G. T., 1975. *Mon. Not. R. astr. Soc.*, **171**, 311.
Bath, G. T., 1976. *Novae and Related Stars,* ed. Friedjung, M., D. Reidel, Dordrecht.
Bath G. T., Evans, W. D., Papaloizou, J. C. B. & Pringle, J. E., 1974. *Mon. Not.R. astr. Soc.*, **169**, 447.
Córdova, F. A., Nugent, J. J., Klein, S. R. & Garmire, G. P., 1980a. *Mon. Not. R. astr. Soc.*, **190**, 87.
Córdova, F. A., Mason, K. O. & Nelson, J. E., 1980b. *Astrophys. J.*, in press.
Kiplinger, A. L., 1980. *Astrophys. J.*, **236**, 839.
Lightman, A. P., 1974a. *Astrophys. J.*, **194**, 419.
Lightman, A. P., 1974b. *Astrophys. J.*, **194**, 429.
Lin, D. N. C. & Pringle, J. E., 1976. *IAU Symp. 73, Structure and Evolution of Close Binary Sysems,* eds Eggleton, P. P., Milton, S. & Whelan, J. A. J., D. Reidel, Dordrecht.
Lubow, S. H. & Shu, F. H., 1975. *Astrophys. J.*, **198**, 383.
Lynden-Bell, D., 1969. *Mon. Not. R. astr. Soc.*, **142**, 505.
Lynden-Bell, D. & Pringle, J. E., 1974. *Mon. Not. R. astr. Soc.*, **168**, 603.
Mayo, S. K., Wickramasinghe, D. T. & Whelan, J. A. J., 1980. *Mon. Not. R. astr. Soc.*, **193**, 793.
Papaloizou, J. C. B. & Bath, G. T., 1975. *Mon. Not. R. astr. Soc.*, **172**, 339.
Papaloizou, J. C. B. & Pringle, J. E., 1977. *Mon. Not. R. astr. Soc.*, **181**, 441.
Pringle, J. E., 1976. *Mon. Not. R. astr. Soc.*, **177**, 65.
Pringle, J. E., 1977. *Mon. Not. R. astr. Soc.*, **178**, 195.
Pringle, J. E. & Savonije, G. J., 1979. *Mon. Not. R. astr. Soc.*, **187**, 777.
Shakura, N. J. & Sunyaev, R. A., 1973. *Astr. Astrophys.*, **24**, 337.
Williams, R. E., 1980. *Astrophys. J.*, **235**, 939.
Wood, P. R., 1977. *Astrophys. J.*, **217**, 530.
Zuckermann, M. C., 1962. *Ann. Astrophys.*, **24**, 431.